VI International Conference on Particle-based Methods – Fundamentals and Applications
PARTICLES 2019
E. Oñate, M. Bischoff, D.R.J. Owen, P. Wriggers & T. Zohdi (Eds)

A CONSISTENT BOUNDARY METHOD FOR THE MATERIAL POINT METHOD – USING IMAGE PARTICLES TO REDUCE BOUNDARY ARTEFACTS

STEPHAN SCHULZ[1], GODEHARD SUTMANN[1,2]

[1] Interdisciplinary Centre for Advanced Materials Simulation (ICAMS)
Ruhr-University Bochum
D-44801 Bochum, Germany
e-mail: stephan.schulz-x2q@rub.de, web page: http://www.icams.de

[2] Jülich Supercomputing Centre (JSC)
Forschungszentrum Jülich GmbH
D-52425 Jülich, Germany
e-mail: g.sutmann@fz-juelich.de - Web page: http://www.fz-juelich.de

Key words: material point method, particle methods, boundary conditions, materials science, Euler-Lagrangian method

Abstract. The Material Point Method (MPM) is a continuum-based numerical method which discretises the object as material points. It is particularly well suited for and has shown great success in the community for large deformations. Even though it has been widely adopted, there are still fundamental questions to be addressed.

In MPM the material properties are carried on the material points and the dynamics is calculated on an overlaid grid. Afterwards, the material points are integrated according to the grid values using an explicit time integration scheme. The explicit boundary methods are applied on the grid values, such as setting the grid momentum to zero for grid nodes inside a fixed wall. This can cause artefacts in the stress as seen for an object in touch with the wall. These distort the stress multiple grid lengths into the object.

In this paper we propose a novel consistent boundary method to reduce these artefacts. The method is based on image particles, an approach originally developed for electrostatic problems. This concept allows a consistent formulation for the momentum field on both the grid and particles. We demonstrate a way of optimization that makes the explicit construction of mirror particles unnecessary.

The explicit boundary method and image particle method are then compared using numerical examples featuring stress induced by simple shear and body forces.

These numerical examples show a significant reduction of boundary artefacts using the image particle method.

1 INTRODUCTION

Materials science simulations have evolved into a powerful branch which complements experiment and theory and provides additional insight into, e.g., structure and mechanical properties on different length scales. On the macroscopic level, continuum methods based on Eulerian methods, e.g., finite element techniques (FEM) had a great success in describing mechanical, thermodynamic or elasto-plastic properties of materials. Alternatively, Lagrangian methods, e.g., smoothed particle hydrodynamics (SPH) have been adopted to overcome the computational overhead in administrating complex meshes in system set ups, involving either complex geometries or time dependent deformation [1], and presenting an alternative approach to FEM. However, problems in terms of momentum and/or energy conservation, appearance of dynamical artefacts or computational overheads due to neighbour searches poses, for certain simulation scenarios, limits on quantitative comparison with, e.g., FEM. To overcome in part some problems of SPH and to improve some features of FEM, an alternative approach, the materials point method (MPM), has been suggested, which is an Eulerian-Lagrangian method, i.e., transporting physical properties in time on particles but performing computations on a mesh. This approach gains flexibility in adjusting to complex scenarios by self adaptation through the use of particles and avoiding the need of re-meshing the computational grid in cases of large deformation by filling the space with particles, which are mapped onto a regular mesh, that is simple to administrate. Since its development, the method has been applied to a growing number of application scenarios.

For simulations of deformations, MPM has been applied to systems, such as snow [2], foam [3] or sand [4]. It has also been applied to cold spraying of particles [5], simulation of tunnelling induced deformations [6], sliding contact ploughing [7] or micro milling [8].

MPM originates from fields of particle simulation methods, applied to systems where the detailed short range nature of interactions is coarse grained and known as Particle In Cell (PIC) method [9]. A number of variants were later on developed which were based on similar assumptions, but modified details to better conserve quantities, e.g., energy, momentum or angular momentum. E.g., the Fluid Implicit Particle (FLIP) method consists of a modification to better simulate fluids [10]. For materials science, MPM was the first approach to solve the specific underlying equations on the continuum level [11], which was later on improved by versions respecting rotational invariants (RPIC) or affine fields (APIC) [12]. Although, MPM as been further developed towards an alternative to FEM, some problems have still not been sufficiently considered and are often suppressed in discussions about the method. One important aspect is the consistent treatment of boundary conditions, which affect slip-, no-slip or prescribed force- or velocity boundary conditions. E.g., in the stress field of a material, often an artificial oscillatory behaviour is observed, which might lead to instabilities or error propagation. The present article is a contribution to increase awareness to this type of artefacts in MPM and to provide a method to avoid such artefacts in materials simulations.

2 THE ALGORITHM

We are using the APIC method by Jiang et al. [12] and Jiang, Schroeder, and Teran [13] with a few additions shown in this section and explicit time integration.

The simulation is initialised with the particles and their corresponding material properties. First the momentum is transferred onto the grid. Then the internal state, the strain and deformation gradient, as well as stress of the particles, is updated followed by the internal forces based on the particles' stress and external forces. The resulting forces on the grid are then used to integrate the momentum of the grid nodes calculating the dynamics. These are then transferred back onto the particles and their velocities, positions, strains, deformation gradients are updated, propagating the material properties. Boundary conditions are omitted here, because they are described later in subsection 2.3.

In the following we will index quantities on nodes with i and on particles with p. If all variables of an equation are from the same time step n it will be omitted.

2.1 Damped dynamics

In some cases a fully dynamic simulation is unnecessary and can lengthen the simulation time needed to reach equilibrium, if at all possible. For these cases we implement a simple reduction of dynamics by dissipating the kinetic energy in every time step. This is done by setting the grid momentum to zero after transferring the particle properties to the grid. The following integration is then just a relaxation of the particles along the gradient of the force.

2.2 Force description

To apply forces on (selected) particles an acceleration is applied. The total force is thereby given as

$$\boldsymbol{F} = \int \rho\, \boldsymbol{b}\, \mathrm{d}V \tag{1}$$

$$= \sum_p m_p \boldsymbol{b}_p \tag{2}$$

$$= \sum_{i,p} m_p \boldsymbol{b}_p w_{ip}. \tag{3}$$

For a constant acceleration $\boldsymbol{b}_p$ and particle mass m_p this results in

$$\boldsymbol{F} = N_p m_p \boldsymbol{b}_p. \tag{4}$$

Here ρ is the mass density and $\boldsymbol{b}$ acceleration of the material. Because the acceleration $\boldsymbol{b}_p$ is weighted by the particle mass, the resulting force is independent of the number of particles and only depends on the total mass of the accelerated object.

2.3 Boundary conditions

When simulating most systems, their boundaries must be treated specifically. For some we prescribe a desired velocity, for others a certain force acting on objects on contact with

the boundary. Here we will focus on no-slip boundaries, where no relative motion is desired between the boundary and objects in touch with it, slip boundaries, where only motion parallel to the boundary is desired and a force based boundary, that also applies a certain force on the object in contact.

We will see that the commonly used boundary conditions induce stress artefacts as visible in Figure 1 for example. In section 3 we investigate the artefacts closer for two example set ups.

2.3.1 Explicit no-slip

To apply the no-slip boundary a straightforward method is to set the node momentum and acceleration of nodes within the boundary to zero [14]. It is important to not only set $\boldsymbol{q}_i = \mathbf{0}$ after the particle to grid transfer, but also to set the total force $\dot{\boldsymbol{q}}_i = \mathbf{0}$. Otherwise, particles can slowly move into the boundary under a continuous force.

2.3.2 Explicit slip

To enforce full slip boundaries a similar method is used, but only the momentum and acceleration perpendicular to the boundary are set to 0. So for a boundary with the normal $\hat{\boldsymbol{n}}$ we modify the momentum as

$$\boldsymbol{q}' = \boldsymbol{q} - \boldsymbol{q}_\perp (= \boldsymbol{q}_\parallel) \tag{5}$$

$$= \boldsymbol{q} - \hat{\boldsymbol{n}}(\hat{\boldsymbol{n}} \cdot \boldsymbol{q}). \tag{6}$$

2.3.3 Boundary object

The image particle treatment as described above does not include additional external forces or a force based boundary. What we can do instead is use a boundary layer of particles which are accelerated and have no slip with regards to the original object. The boundary layer should have a certain thickness and can also be wider than the object. Note, since the boundary is defined using the acceleration of the boundary layer particles, the thickness and width changes the total force acting on the object. Care must be taken when setting up the system to get the desired forces.

2.3.4 Image particles

When running simulations using the above mentioned boundary conditions certain artefacts appear in the stress distribution as visible on the left in Figure 1. To mitigate these artefacts we propose a new method to implement boundary conditions.

This new method originates from electrostatics and is known as image charges [15]. Mirroring an electric charge on a plane with a sign change causes a constant electric field of $0\,\mathrm{V\,m^{-1}}$ at the plane. The same can be done for the particles' properties in MPM.

For a particle shown as a cross in Figure 2 near a planar boundary, we create an image particle at the same distance on the opposite side of the wall. With the vector $\boldsymbol{d}$

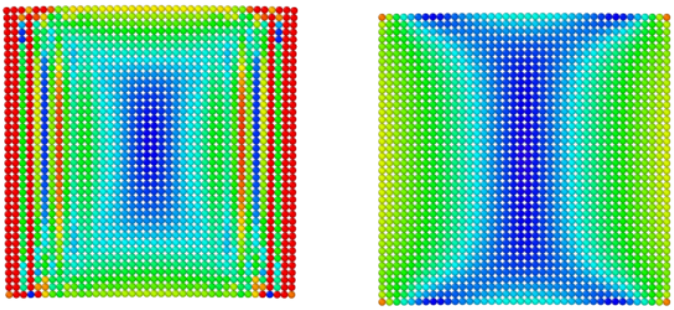

Figure 1: An example of the artefacts introduced by the explicit boundary conditions. The left figure shows the von Mises stress for the explicit boundary conditions and the right figure with the proposed image particle method. This set up is further investigated in section 3.

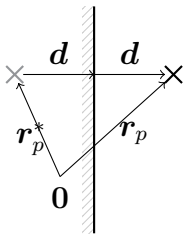

Figure 2: The particles and its image counterpart are separated by $2\boldsymbol{d}$. That vector is perpendicular to the boundary. An arbitrary origin $\mathbf{0}$ is shown in the figure.

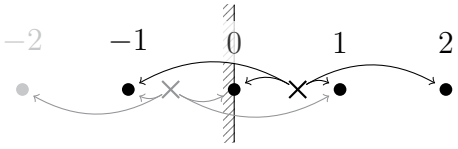

Figure 3: Shown are a particle (black cross) its virtual counterpart (grey cross) the grid nodes (circles) and to which grid nodes quantities are contributed. The light grey grid node does not contribute to the original particle and can be ignored.

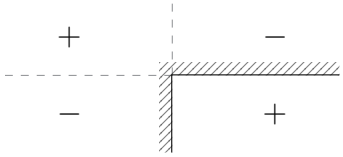

Figure 4: The sign changes of the mirrored quantities are shown for a positive quantity in the lower right quadrant. Each mirroring changes the sign.

describing the shortest distance from the boundary to the particle at $\boldsymbol{r}_p$ the image particle is positioned at

$$\boldsymbol{r}_p^* = \boldsymbol{r}_p - 2\boldsymbol{d}. \tag{7}$$

This process has to be repeated for each boundary, as seen in Figure 4. The particle is represented with a positive quantity in the lower right quadrant. It is then mirrored to the lower left quadrant with a negative quantity. For multiple boundaries we have to mirror image particles as well. So both of these particles are then mirrored into the upper quadrants with their respective sign changes. The order of the mirroring does not change the result, but for clarity we are first treating x direction, then y and lastly z.

A particle with respect to the grid nodes is shown in Figure 3. We see the four nodes to which properties are transferred to, indicated with black arrows. The nodes $i \leq 0$ are boundary nodes. Node -2 can safely be ignored, because it does not transfer its

quantities onto any real particles, if we assume the material stays outside the boundary. The contributions of the image particles are shown with grey arrows.

The purpose of this set up is to reach a no-slip condition at the boundary, which means the momentum and force of the boundary node should be 0. The question arises, if we can simply change the sign of the properties that are being transferred. The desired result is, that the contribution of the particle to grid node i is counteracted by the image particles contribution. In the case of the grid momentum a change of sign in the particle velocity almost suffices as can be seen from the particle to grid transfer of the momentum

$$\boldsymbol{q}_i = \sum_p w_{ip} m_p \boldsymbol{v}_p + \sum_p w_{ip} m_p \mathbf{B}_p (\mathbf{D}_p)^{-1} (\boldsymbol{r}_i - \boldsymbol{r}_p). \tag{8}$$

In the case of APIC the affine matrix $\mathbf{B}_p$ has to be treated as well. For this we look at the behaviour when the relative position $\Delta \boldsymbol{r}_{ip}$ changes sign in one component. The transfer function is symmetric, so

$$w_{ip} = w^*_{ip}. \tag{9}$$

Mirrored properties will be indexed with a star. The second term of the momentum contains $(\boldsymbol{r}_i - \boldsymbol{r}_p)$ $(= -\Delta \boldsymbol{r}_{ip})$ which changes sign only in the component the particle is mirrored against. This means the affine matrix has to change in all columns except the one we mirror in. Using Greek indices for the components and the Kronecker delta we can write this as

$$B^*_{p,\alpha\beta} = -B_{p,\alpha\beta} + 2B_{p,\alpha\beta}\delta_{\beta\kappa} \tag{10}$$

for the mirror direction κ. The mass will be untouched and the particle acceleration can simply change its sign.

As an example let's mirror in the y direction, so $\kappa = 2$. Then we have

$$\Delta \boldsymbol{r}^*_{ip} = \begin{pmatrix} \Delta r_{ip,1} \\ -\Delta r_{ip,2} \\ \Delta r_{ip,3} \end{pmatrix} \tag{11}$$

and the mirrored affine matrix must be constructed as

$$\mathbf{B}^*_p = \begin{pmatrix} -B_{p,11} & B_{p,12} & -B_{p,13} \\ -B_{p,21} & B_{p,22} & -B_{p,23} \\ -B_{p,31} & B_{p,32} & -B_{p,33} \end{pmatrix} \tag{12}$$

so the resulting mirrored velocity is

$$\boldsymbol{v}^*_p = -\boldsymbol{v}_p. \tag{13}$$

The treatment of the particle state, that will result in the opposite internal force contribution, is more complex. Even for the simple Hooke's Law this is not necessarily easy. However, in general we have to invert the constitutive equation to know how to

transform the strain or deformation gradient. This follows from the definition of the internal force on the grid nodes

$$\boldsymbol{f}_i^{(\mathrm{i})} = -\sum_p V_p \sigma_p \cdot \boldsymbol{\nabla} w_{ip} \tag{14}$$

where the particle stress is used to calculate the internal force. To see how the stress has to transform we first look at the transfer function gradient. Similar to the relative distance earlier only the component of mirroring changes sign. The internal force is the dot product of the stress and the gradient, so, as with the affine matrix, all components of the stress not inverted by the transfer function gradient have to be inverted. This means

$$\sigma^*_{p,\alpha\beta} = -\sigma_{p,\alpha\beta} + 2\sigma_{p,\alpha\beta}\delta_{\beta\kappa}. \tag{15}$$

For a Poisson ratio of 0 and Hooke's Law this applies to the strain as well, since it is a linear relationship.

Luckily, the exact properties of the image particle are not needed, because we only need the contributions of it. This means we can simply calculate the contributions of our particle and add the negative of those to the appropriate grid nodes the image particle would transfer to. For this to work we have to assume the transfer function has the same value for both particle node pairs. This is only given if the particle is mirrored exactly at a plane parallel to two axes and aligned on the node positions. Taking Figure 3, the transfer function between the particle and node 0 is then the same as between the image particle and node 0. The same holds between the particle and node 1, and the image particle and node -1.

Image charges work, because of the anti symmetry in the resulting field. This ensures the field at the boundary, the symmetry plane, is always zero. If a second plane is introduced, a second boundary, it must also be anti symmetric to the first plane. This can only be satisfied for a perpendicular plane. Therefore, complex boundaries are not supported, but only boxes.

Unaligned boundaries are also possible, albeit with a bit more computational effort. Assuming unaligned boundaries that are still parallel to the axis planes, instead of just adding the corresponding value of the particle to the image particles grid node, the weight is recalculated. So the particle property has to be reused at a new position, the mirror particle's position. This means additional evaluation of the transfer function and its gradient. This also causes additional bookkeeping effort for the caching of these values as is done for the normal particles as well.

3 THE SIMULATION SET UP

We will consider two types of boundaries. First, no-slip boundaries where the material should not move relative to the boundary. Second, slip boundaries with a constant force acting on the material parallel to the boundary. In both cases the boundary itself is fixed. The simulations are done in three dimensions with the material block as a cube. The relevant simulation parameters are shown in Figure 1. These parameters result in

64 000 particles. The method supports a wide variety of constitutive equations for the material, such as neo-Hookean, or Drucker-Prager based elastoplastic [4] materials. Only the calculation of the internal force is needed, for which the stress of the particle is used. Here we will use Hooke's Law to calculate the stress from the strain

$$\sigma = \mathbf{C}\varepsilon \tag{16}$$

with the stiffness tensor $\mathbf{C}$. The Young's modulus Y and Poisson ratio ν are used as material properties.

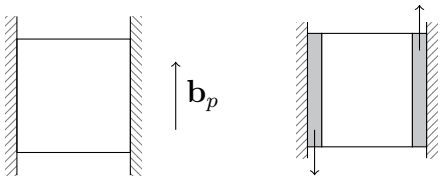

Figure 5: On the left a body force is acting on the material and the left and right walls are no-slip. On the right a simple shear is created by applying a constant force to the left and right boundary layers. The two walls are full slip.

Table 1: Simulation parameters used for the example set ups.

Δt	$1 \times 10^{-4}\,\mathrm{s}$
Δh	$0.05\,\mathrm{m}$
N_p/cell	8
Y	$1 \times 10^{4}\,\mathrm{Pa}$
ν	0
L	$1\,\mathrm{m}$
b_p	$100\,\mathrm{m\,s^{-2}}$
$\lvert b_{p,\mathrm{boundary}}\rvert$	$400\,\mathrm{m\,s^{-2}}$
L_{bd}	$0.5\Delta h$

For comparisons, we will look at the von Mises stress defined as

$$\sigma_v = \left(\frac{1}{2}\left((\sigma_{xx}-\sigma_{yy})^2 + (\sigma_{yy}-\sigma_{zz})^2 + (\sigma_{zz}-\sigma_{xx})^2\right) + 3\left(\sigma_{xy}^2 + \sigma_{yz}^2 + \sigma_{zx}^2\right)\right). \tag{17}$$

3.1 No-slip boundary

In the first case we induce a strain in the material by applying a constant acceleration $\boldsymbol{b}_p$ parallel to the boundary as seen on the left in Figure 5. The left and right boundaries should result in no-slip and the other boundaries are open.

Using the explicit no-slip boundary conditions from subsubsection 2.3.1, the stress shows very large oscillations at the no-slip boundaries on the left and right. The resulting von Mises stress distribution is shown in Figure 6 on the left. These oscillations are quite wide and reach multiple grid widths into the material. In these simulations the particles are half a grid width apart.

These oscillations are on the length scale of a few grid widths which can be seen for a higher resolution simulation in the second image of Figure 6. There the same set up has been used, but the grid width was reduced by a factor of five to $\Delta h = 0.01\,\mathrm{m}$, resulting in 8 000 000 particles. The stress distribution is now correctly modelled inside the object, but due to the additional computation time reducing the grid width not a valid option.

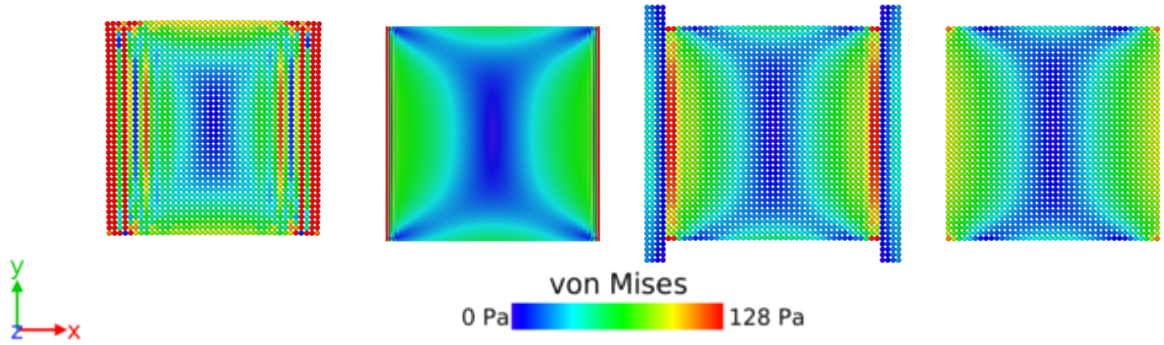

Figure 6: The no-slip set up for the different boundary conditions. From left to right they are the explicit method in normal and higher resolution and a boundary object, followed by our proposed image particle method. The boundary artefacts appear on the length scale of grid widths at the left and right boundary. For the image particle method only small artefacts in the corners are visible.

These artefacts are reduced if a buffer object is introduced between the material and the boundary as shown in the third image of Figure 6. Here the buffer object is two grid widths deep, which equals the penetration of the used transfer function. A very clear difference to the unbuffered method is also visible at the top and bottom boundaries. Except for the one grid width wide area at the left and right boundary, the expected stress is computed quite well. The drawback for this method is the additional computational effort for the buffer objects, which is non negligible.

These artefacts are further reduced with our image particle method from subsubsection 2.3.4. The result is shown on the right in Figure 6. No artefacts can be seen at any boundary. Only the corners show an aberration as small as a grid cell. Although the image particles require additional computational effort as well, with optimizations this can be very small and limited to simple additions.

Another aspect of interest is the time the simulations take to reach a steady state. The explicit boundary condition has not converged after 1000 time steps (0.1 s), with the main change still occurring in the boundary region of large artefacts. The buffer objects decreases this time to about 250 time steps (0.025 s), whereas the image particles cause a fast convergence in about 100 time steps (0.01 s).

The run time of these simulations shows the inefficiency of the buffer object method. That method took about 50 % longer to run than the explicit method. This is mainly caused by the introduction of new particles by the buffer object, which actually are not needed for the image particles, since we just duplicate the transfer from particle to grid. The difference of run time between the image particle method and the explicit method is within the margin of error.

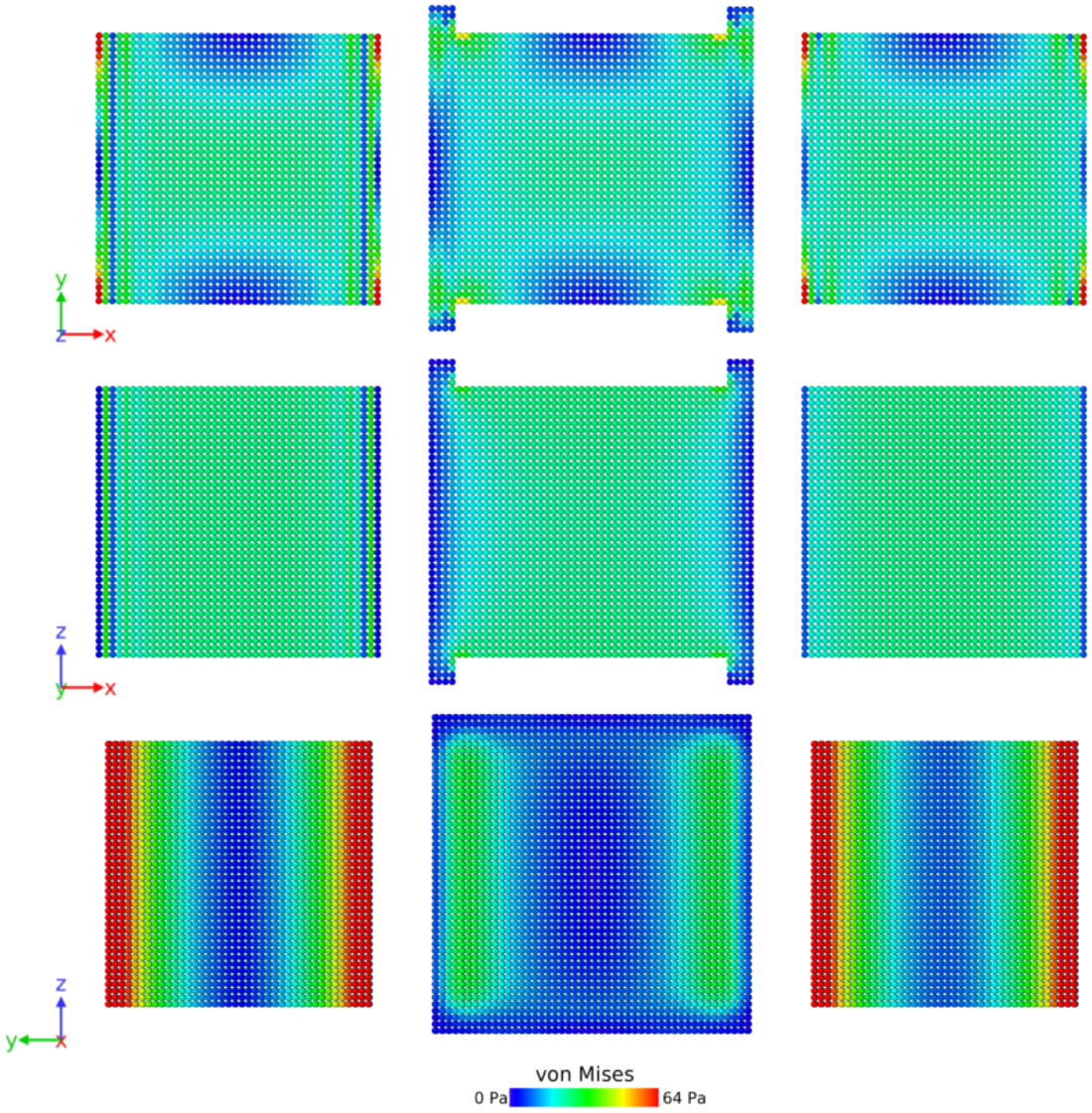

Figure 7: Three methods are shown in columns. The first two are the explicit method with a single and respectively four particle layer boundary object. The last one also has a single layer boundary object, but uses the image particle method. The rows show different views of the stress distribution of the systems. The first row shows the stress in the middle of the system with the external shear forces applied on the left and right towards positive and negative y direction. The second row has the forces on the left and right into and out of the page. The last row shows the boundary layer from the left.

3.2 Constant force boundary

To study force based boundaries a simple shear set up as shown in Figure 5 on the right is used. The shear is induced by an acceleration $\boldsymbol{b}_p$ acting on the object between the material and the slip boundary.

For a boundary object with one particle thickness the von Mises stress is shown in the first column of Figure 7. The artefacts from the no-slip case are much less pronounced, but still visible. They also still reach a few grid widths into the material.

For an increased thickness of the boundary object of two grid lengths, the depth of the transfer function, we see much less of the oscillating artefacts. The results are shown in the second column in Figure 7. The stress distribution is smooth inside the material and across into the boundary object. The edges along z direction show up in the upper figure in the corners as yellow. The stress is, however, much improved compared to the thin object. Due to the larger boundary object, this simulation takes about 23 % longer to run. However, the image particle method and explicit method have about the same run time.

The boundary artefacts can also be reduced by using the image particle method, modified to provide a slip boundary, and a one particle boundary layer. This results in the stress shown on the right in Figure 7. The artefacts are much smaller than for the explicit boundary method, but still more pronounced than for the thick boundary object.

In other particle based simulation methods, such as SPH, similar boundary effects are observed as have Ma and Hartmaier [1].

4 CONCLUSION AND FURTHER WORK

We have shown that the image particle method efficiently removes the high frequency boundary oscillations in the stress for a no-slip and slip boundary. In a simple shear set up induced by boundary objects with forces, the stress field is more accurately represented than in the case of the normal boundary condition. Although small artefacts remain in the extreme case of a thin, one particle layer, boundary object.

The image particle method can be highly optimized for planar boundaries aligned with node positions. Unaligned boundaries are also possible, but require additional computational effort, chiefly because the transfer weights have to be recomputed.

An additional force acting directly on the image particles and propagating onto the grid is easy to implement, but more difficult to control. The total force acting on the system depends on both the volume of image particles and whether the grid nodes onto which the image particles contribute to, have an effect on real particles.

The method shown does not include boundaries with a limited extent, but assumes unbounded planes. It can also be adapted for walls and boundaries with limited extent, but a few additional considerations have to be made. Further work into this direction will be conducted, since it is required for the simulation of more complex environments, such as equal channel angular pressing. Furthermore, the parameters such as the thickness and extent of the boundary object can be further optimized.

References

[1] Ma, A. and Hartmaier, A. A crystal plasticity smooth-particle hydrodynamics approach and its application to equal-channel angular pressing simulation. *Model. Sim. Mat. Sci. Eng.* **24** (2016), 085011.

[2] Stomakhin, A., Schroeder, C., Chai, L., Teran, J., and Selle, A. A material point method for snow simulation. *ACM Trans. Graph.* **32** (2013), 102.

[3] Ram, D., Gast, T., Jiang, C., Schroeder, C., Stomakhin, A., Teran, J., and Kavehpour, P. A material point method for viscoelastic fluids, foams and sponges. *Proceedings of the 14th ACM SIGGRAPH/Eurographics Symposium on Computer Animation*. ACM. 2015, 157–163.

[4] Klár, G., Gast, T., Pradhana, A., Fu, C., Schroeder, C., Jiang, C., and Teran, J. Drucker-prager elastoplasticity for sand animation. *ACM Trans. Graph.* **35** (2016), 103.

[5] Liu, Y. and Xu, C. Investigating the cold spraying process with the material point method. *Int. J. Mech. Mat. Design* **15** (2019), 361–378.

[6] Fern, E. J. Modelling tunnel-induced deformations with the material point method. *Comp. Geotechnics* **111** (2019), 202–208.

[7] Mishra, T., Ganzenmüller, G. C., Rooij, M. de, Shisode, M., Hazrati, J., and Schipper, D. J. Modelling of ploughing in a single-asperity sliding contact using material point method. *Wear* **418** (2019), 180–190.

[8] Leroch, S., Eder, S., Ganzenmüller, G., Murillo, L., and Ripoll, M. R. Development and validation of a meshless 3D material point method for simulating the micro-milling process. *J. Mat. Proc. Tech.* **262** (2018), 449–458.

[9] Harlow, F. H. The Particle-In-Cell Method for Numerical Solution of Problems in Fluid Dynamics. *Experimental Arithmetic, High Speed Computing and Mathematics*. American Mathematical Society, 1963, 269–288.

[10] Brackbill, J. U., Kothe, D. B., and Ruppel, H. M. FLIP: a low-dissipation, particle-in-cell method for fluid flow. *Comp. Phys. Commun.* **48** (1988), 25–38.

[11] Sulsky, D., Zhou, S.-J., and Schreyer, H. L. Application of a particle-in-cell method to solid mechanics. *Comp. Phys. Commun.* **87** (1995), 236–252.

[12] Jiang, C., Schroeder, C., Selle, A., Teran, J., and Stomakhin, A. The affine particle-in-cell method. *ACM Trans. Graph.* **34** (2015), 51.

[13] Jiang, C., Schroeder, C., and Teran, J. An angular momentum conserving affine-particle-in-cell method. *J. Comput. Phys.* **338** (2017), 137–164.

[14] Buzzi, O., Pedroso, D. M., and Giacomini, A. Caveats on the implementation of the generalized material point method. *Comp. Model. Eng. Sci.* **31** (2008), 85–106.

[15] Jackson, J. D. *Classical Electrodynamics*. 3rd ed. Wiley, 1998.